Journal of Nuclear Materials 390–391 (2009) 852–857

Contents lists available at ScienceDirect

Journal of Nuclear Materials

journal homepage: www.elsevier.com/locate/jnucmat

Impact of lithium-coated walls on plasma performance in the TJ-II stellarator

J. Sánchez, F.L. Tabarés *, D. Tafalla, J.A. Ferreira, I. García-Cortés, C. Hidalgo, F. Medina, M.A. Ochando, M.A. Pedrosa, The TJ-II Team

Laboratorio Nacional de Fusión, CIEMAT, Avenida Complutense 22, 28040 Madrid, Spain

ARTICLE INFO

PACS:
28.52.−s
28.52.Fa
52.55.Hc
52.40.Hf

ABSTRACT

Lithiumization in the TJ-II heliac has been recently performed by vacuum evaporation of metallic Li. Compared to previous wall coating scenarios, an enhanced density control by external puffing and discharge reproducibility, leading to the drastic enlargement of the operational window, has been obtained for hydrogen and helium plasmas. Strong changes in recycling, impurity composition, edge radiation profiles and global energy confinement have been recorded. The long-lasting effect of the new coating extends to H-wall inventories beyond the expected saturation of the Li layer by particle implantation. Sputtering yields for Li much lower than bibliographic values were measured. These changes had also impact on the plasma profiles under NBI heating scenarios, with increased peaking of the electron density profiles and fuelling rates corresponding to the nominal beam current. Strong ELM-type activity was seen, associated to significant changes in edge fluctuation levels and the presence of steep gradients in edge parameters.

1. Introduction

In the last years, lithium wall conditioning has been carried out in several fusion devices (Tokamaks, Compact Toruses) by different techniques, providing in many instances record values of plasma parameters and enhanced plasma reproducibility [1–4]. Thus, TFTR achieved the highest values in D–D neutron rates (super shots) by Li pellet injection into the plasma [1], and enhanced confinement regimes were observed in the Li tray experiments in CDX-U [2]. The Capillary Porous System has been implemented with success in the T-11 M and FTU tokamaks [3,4], opening the possibility of developing high radiative, low recycling liquid divertor concepts of high potential for future reactors [5]. Behind these findings are the low recycling, low contamination and non-coronal enhanced radiative power dissipation properties of Li.

Compared to tokamaks, stellarator plasmas show a distinct impact of plasma-wall interaction processes on plasma performance. The lack of disruptions and Type-I ELMs make them more reliable for reactor operation. So it is the lack of MHD-driven density limit. However, no specific coating strategies for the first wall have been developed. Application of the successful concepts for tokamaks, such as boronization or Ti gettering, has also improved machine operation in the stellarator community [6]. Moreover, the intrinsic radiative character of the density limit of stellarators [7] makes wall-material exchange experiments highly relevant for the benchmarking of running models. In the present work, the plasma performance of the TJ-II Heliac under lithium-coated wall conditions with lithium is described for the first time in a stellarator. Compared to previous coatings, lithium has produced the best plasma performance to date, leading to the achievement of record values in plasma density and energy confinement. In the present work, we shall focus on the impact of the Li coating operation on edge characteristics and plasma-wall interaction issues.

2. Wall conditioning of the TJ-II stellarator

To date, three different first wall scenarios have been investigated in TJ-II [8], requiring the implementation of several conditioning techniques. For the initial scenario, a full metal machine, desorption of high recycling He from the walls, which was implanted during overnight GD conditioning, either by the plasma or by direct interaction with the microwave beams was the main responsible for problematic density excursions. The systematic use of a short Ar GD period led to a significant improvement of the control. Under boronized walls and graphite limiters (low Z scenario), the improvement in plasma purity and the low recycling conditions at the beginning of the operation (shortly after the depletion of H from the film by He GD) provided a higher tolerance of the plasma to the external fuelling [9]. However, two complications were found under boronized walls. First, the gradual loading of the C/B film by hydrogen deteriorates the good recycling characteristics in a relatively short period. After a total implantation dose corresponding to the maximum uptake of the film of

* Corresponding author.
E-mail address: tabares@ciemat.es (F.L. Tabarés).

0022-3115/$ - see front matter © 2009 Elsevier B.V. All rights reserved.
doi:10.1016/j.jnucmat.2009.01.224

$\sim 1 \times 10^{17}$ cm^{-2} was achieved, spontaneous density rise drove the discharge to cut-off density, even in the absence of external puffing. The application of a few dry discharges was required for recovery, but this was only transiently obtained. A second factor in play was the presence of the Enhanced Particle Confinement (EPC) mode, characterized by a sudden increase of particle confinement at a critical density in the order of 0.6×10^{19} m^{-3} [10]. Transition into this mode was found to strongly depend on fuelling pulse shape and amplitude [11] and, its development can be eventually suppressed by proper tailoring of the gas puffing.

Finally, in the 2007 campaign, the inner walls were boronized and then covered by lithium. For that purpose, an *in situ* lithium coating technique was developed. It is based on evaporation under vacuum from four retractable ovens, symmetrically spaced and oriented tangentially to the radius of the machine (see Fig. 1). Each oven was initially filled with 1 g of metallic Li. A set of metallic resistances (Thermocoax) and thermocouples (K type, two per oven) are operated at pre-programmed temperatures of 500–600 °C by a central, PID-based power supply. Effusion from the ovens creates an atomic beam aiming at the remote region opposed to the corresponding flange. Under HV operation, the mean free path of the Li atoms is long enough to produce a thin layer at the vessel walls located midway between adjacent ovens. The deposition pattern, directly visible in the groove protecting the central coils, matches the line of sight flight of the Li atoms. Alternatively, effusion under a He atmosphere was tried to enhance lateral diffusion of the beam, hence providing a more homogeneous coating of the walls in areas closer to the ovens. A pressure of 10^{-5} mbar was chosen, based on the experimentally determined mean free path for the He–Li system at this pressure, $\lambda \sim 70$ cm and the characteristic length of the vacuum vessel, $V/S \sim 20$ cm (assuming pure cylindrical geometry). To date, the best results (in terms of lifetime of the coating respect to particle recycling control) have been obtained when the ovens are filled with enough Li (6 g each) for the periodic conditioning of the machine during a full experimental campaign. The evaporation of Li in this case is free from the presence of other species coming from the outgassing of the metallic parts of the oven (CO, $CO_2 \times H_2O$, H_2 ...). Due to possible lack of homogeneity in the coating, and in order to extend the lifetime of the Li coating, a ~50 nm boron layer was deposited prior to the evaporation by conventional GD of an o-carborane/He mixture. A pure He GD depleted the B coating of H after its deposition. Also, He GD was applied every day on the Li layer in order to remove hydrogen from the areas not fully covered by the coating. A total of 12 g of Li were evaporated for the ~1200 discharges performed in the last campaign. Visual inspection of the Li deposition pattern after plasma operation indicated that some degree of reposition takes place, thus improving the beneficial effects of the coating.

3. Recycling behavior of H and He on Li walls

A dramatic change of the recycling behavior was observed upon lithiumization of the walls. Compared to former operation on boronized walls, the control of plasma density by external puffing was very much upgraded. The required puffing levels were significantly higher for the same density (by a factor 2–3), and no sign of saturation was observed after a full day of ECRH operation. In order to quantitatively understand this effect, the particle balance in a shot to shot basis was evaluated from the injected hydrogen, and the desorbed one after the plasmas, the latter being measured by an absolutely calibrated mass spectrometer. In Fig. 2, the results for a typical operation day under both types of wall conditions are displayed. Two main differences between B and Li walls are clearly seen from the figure. First, the required particle injection for a given density is systematically higher in the Li case. Second, while the B-wall shows saturation at total retained inventory of $H < 5 \times 10^{20}$ (which, for the nominal saturation level of B films, implies an effective interaction area of less than 1 m^2) no sign of such saturation is seen for values up to four times higher in the Li case. Thus, the estimated concentration of H in the lithium-coated parts of the wall with direct interaction with the plasma at the end of the day can be over 4×10^{17} cm^{-2}. For a density of the layer equal to that of the solid Li and a stoichiometry of 1:1 (H:Li) this figure implies the saturation of ~80 nm, obviously much larger than the expected implantation range of ~200 eV H ions, thus indicating that important diffusion into the bulk is taking place even at low (below the melting point, 180 °C) temperatures. The dynamic behavior of

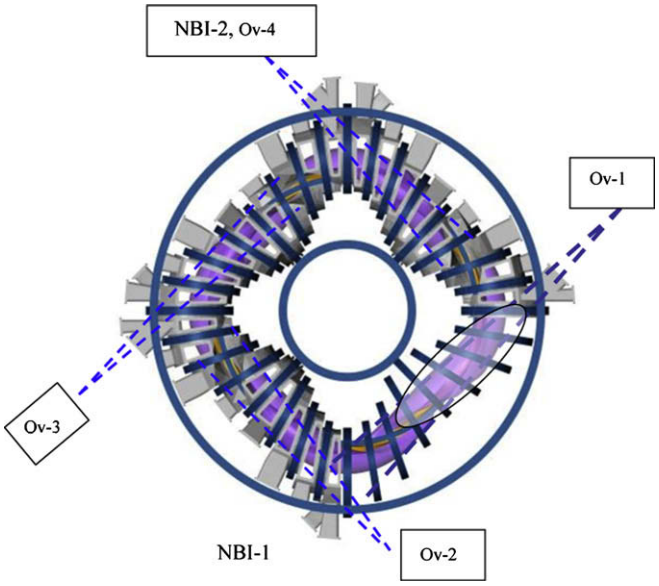

Fig. 1. Top view of TJ-II showing the location of the effusive Li sources. The NBI-2 and the oven #4 share the same injection line. Intersection of the Li beams and the grooved part of the vessel produces an elliptical spot/schematically shown for oven #1).

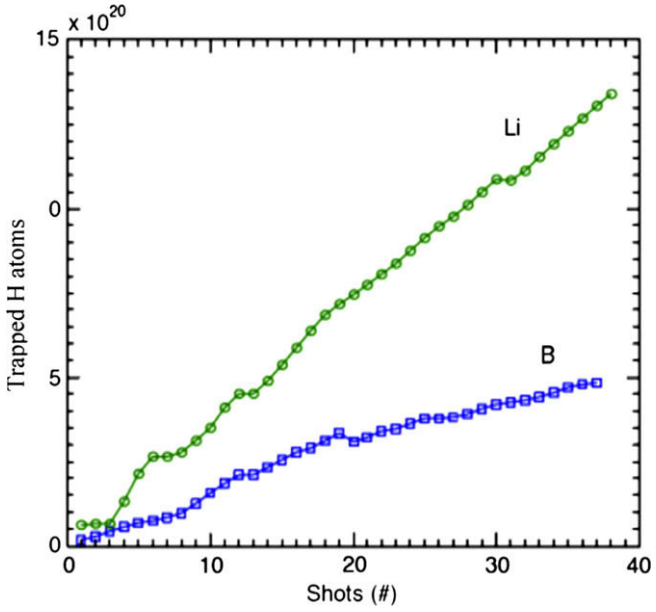

Fig. 2. Cumulative H-wall inventory during an operational day for the B-wall and Li-wall cases.

plasma particles during the discharge is shown in Fig. 3 for a characteristic shot. Examples of H and He plasmas are shown. First, gas puffing is injected for density built up. Then it is abruptly interrupted and the evolution of cord density and Hα emission are recorded. Application of the particle balance equation to the data of Fig. 3(a) (H plasmas) yields a fuelling efficiency near unity and an effective confinement time, $\tau_p/1-R$, of ~8 ms. Assuming no major changes in particle confinement respect to the boron and metal cases (see below), a value of $R < 20\%$ is obtained. This low value, however, still represents an average over the partially covered Li walls, so that even lower values could be achieves under full coating scenarios. Compared to H, He plasmas show a higher recycling, as expected. However, analysis of the density evolution in Fig. 3(b) yield an R value of ~93%. This value evidence that some wall pumping is still present for a typical high recycling impurity under de Li walls. Similar conclusion was drawn from the T-11 M tokamak experiments [3] and opens the possibility of enhancing fusion ash pumping in a future reactor under Li divertor scenarios.

Another important factor contributing to density control by external puffing in the absence of discontinuities in the confinement characteristics, as that introduced by the transition to the EPC mode. This transition correlates with a change in the sign of the perpendicular velocity at the edge, as measured by Langmuir probes [12]. In Fig. 4, the dependence of this velocity at $r = 0.9$ with line average density is shown for the B and Li-wall scenarios. Very similar trends are deduced in both cases, thus indicating that, at least in ECRH plasmas, no major changes in confinement can be ascribed to the new operational regime.

4. Edge parameters and impurity generation

Boronization of TJ-II was aimed at the achievement of clean plasmas, and for the ECRH scenarios this goal wall fulfilled [13]. Under NBI heating, however, plasma collapse was found to take place at densities lower than expected, and therefore operation was limited by density control problems. These problems indeed motivated the lithiumization of the walls. Nevertheless, a significant effect on impurity generation and composition has been observed in that last campaign. So, under ECR heating conditions, carbon and Li emissions together with total radiated power were seen to decrease during the operation day. Fig. 5 shows evolution of some relevant signals, normalized to the line average density for the two first days of operation after Li evaporation. As seen,

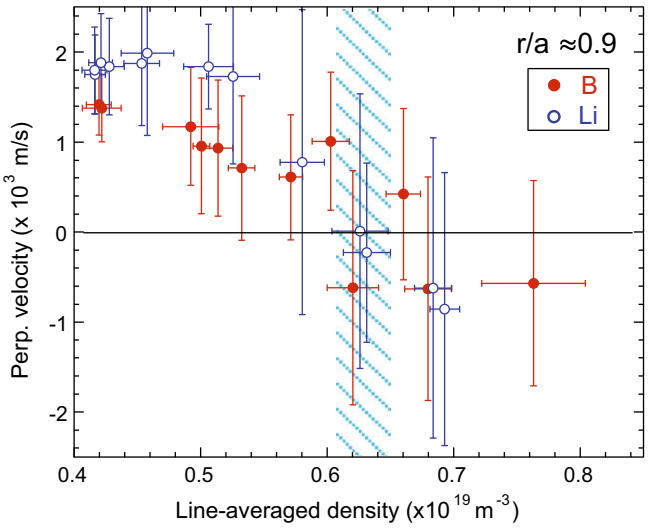

Fig. 4. Evolution of v perpendicular with density for B and Li walls. The density for sign inversion corresponds to the development of the EPC mode.

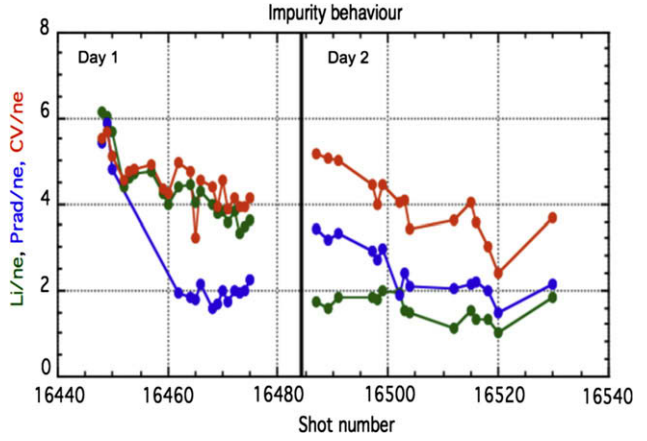

Fig. 5. Impurity evolution during the first two operation days after lithiumization of the walls.

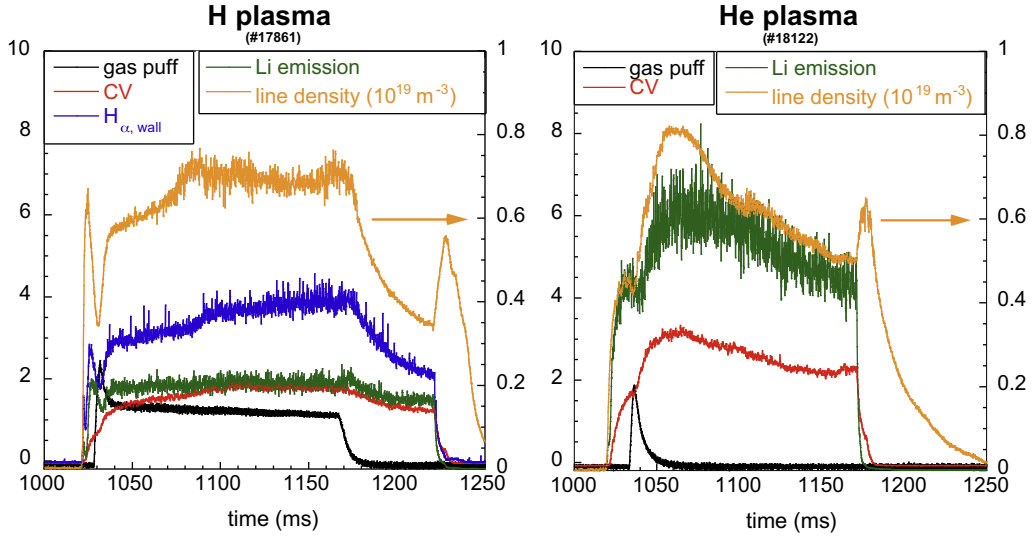

Fig. 3. Recycling characteristics of H and He plasmas under Li-wall operation. Note the higher level of Li and C emissions in the He plasmas.

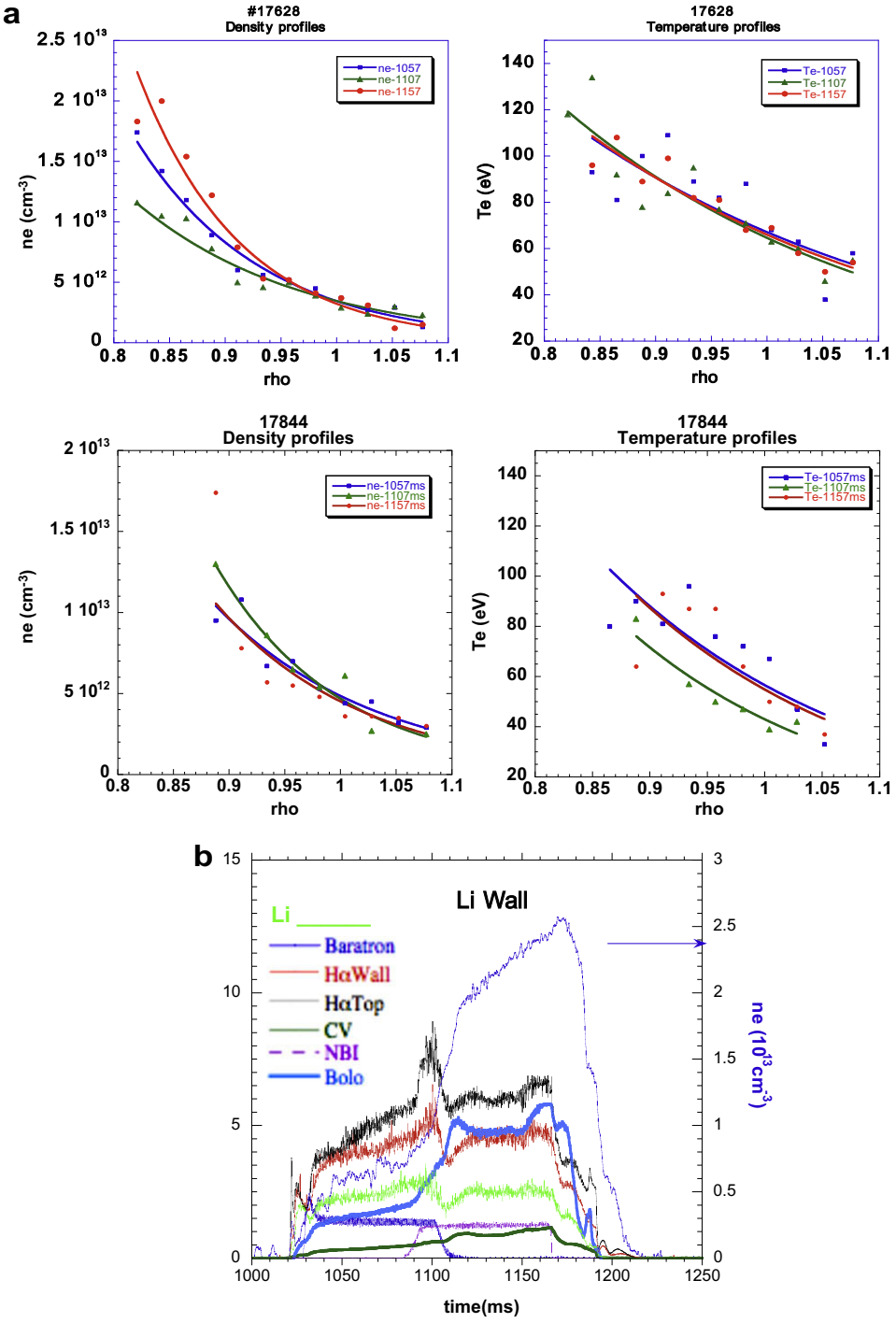

Fig. 6. (a) Edge density and temperature profiles for two NBI plasmas under B-wall (top) and Li-wall (bottom) operation. (b) Evolution of main plasma parameter during a NBI shot under Li-wall conditions. Note the recovering of Hα and Li emission levels in the NBI phase.

after an initial spike in all impurity monitors, associated to the very first shots after Li deposition, a systematic decrease takes place upon plasma operation. Of special relevance is the strong decay of the bolometer signal, closely related to the suppression of carbon impurities from the plasma. The strong reduction of carbon source in the presence of Li is a well documented effect which has been associated to the decrease of physical and chemical sputtering of carbon by its coating with Li [14]. The second day of is preceded by 30 min of He GD. The impurity levels are seen to rise again, but they soon recover to their low levels, the Li signal reaching level up to seven times lower than before. Since its measurement is local, the erosion of the initial layer at the observation window, with subsequent spreading over other areas of the vessel, could account for this effect, in agreement with visual inspection of the initially wetted area. This effect will also account for the concomitant decrease of impurity radiation, not to be expected if simple removal of the beneficial effect was taking place. An estimate of the sputtering yield for the Li coating can be made from the spectroscopic data. The ratio of Li/H fluxes can be deduced from the ratio I:Li (671 nm)/I:Hα after correcting for the S/XB values of the

corresponding lines and recycling factor. A value of $\phi_{Li}/\phi_H \sim 0.44\%$ is directly deduced from bibliographic ion to photon ratio (S/XB) values [15]. Assuming a value of $R = 0.2$, a yield of neutral Li/incident H of 9×10^{-4} is obtained. This is to be compared with the predictions from TRIM codes and other experimental reports. So, in the presence of self-sputtering, this ratio will be given by

$$Li/H = S_H/1 - S'_{ss}, \text{ with } S'_{ss} = S_{ss} - (1 - Rn), \quad (1)$$

where S_H and S_{ss} stands for the sputtering yields of the systems H/Li and Li/Li, respectively and Rn for the reflection coefficient [15,16]. Evaluation of (1) at Te = 50 eV (see below) yields $Li/H_{sputt} \sim 3 \times 10^{-2}$, i.e., more than 30 times higher than the measured value, even when only a 33% of the sputtered Li is assumed to be in its neutral form. Although the reason for this discrepancy is not known, it should be pointed out those binding energies stronger than those deduced from thermodynamic data of solid Li have been recently claimed for the C–Li system [17]. The fact that mixing of the Li and B layers, with the possible incorporation of sputtered C, takes place by plasma erosion and transport during the operation could explain this observation. This could also apply to the initial strong evolution of Li and C radiation displayed in Fig. 5.

The profiles of the edge parameters under B and Li-wall operation, deduced from the supersonic He beam diagnostic, are displayed in Fig. 6(a). Three times are shown, corresponding to the ECRH, the transition (density ramping) and the NBI phases. Arrows in the Fig. 6(b) indicate them. As it can be seen, although electron densities and temperatures at the LCFS are very similar in all cases, both their gradient and time evolution differs. First, Te gradients at the edge are higher in the Li-wall case and, contrary to the B-wall case, a drop in this parameter takes place in the transition (density ramp) phase. Although the density profiles are very similar in the initial, ECRH phase for both scenarios, a continuous rise of the density at $\rho < 0.85$ is seen in the B-wall example. Interestingly, the same profiles are again obtained in the high density, NBI phase for the Li-wall counterpart. These changes reflect the different profiles found across the main plasma by the Thomson Scattering diagnostic and, for the edge, they are also mirrored in the spectroscopic features at the edge (Li and Hα signals), as shown in Fig. 6(b). As a consequence of the constancy in edge parameters after neutral beam injection under Li walls, a strong increase in particle confinement (up to a factor of 5) is deduced for the NBI plasmas.

Impurity radiation profiles are also seen to evolve upon changing the wall material. Two different profile shapes, hereafter referred as bell and dome type, were found to spontaneously develop for the Li-wall scenario. Examples of these profiles and their evolution during a NBI plasma shot are shown in Fig. 7. As seen, absolute central values are higher for bell-shaped profile. The analysis of SXR emission profiles indicates central values of Zeff higher for this type of profile. A strong reduction of the O content in the plasma was deduced from SXR analysis, so that a likely candidate for central plasma contamination is the sputtered carbon from the graphite plates protecting the vessel along the NBI path. The second type, dome-shaped, is only developed for lithiated walls, and implies a significant screening of impurities. Both profiles are mirrored in the Thomson Scattering and SXR tomography data (not shown). At this stage, no critical parameter has been found to trigger any particular profile shape. In spite of their higher total radiation losses, it was found that peaked (bell) profiles are able to withstand higher total radiation levels before plasma collapse. As seen in the figure, the edge emissivities remain low during the density rump-up phase for the bell profiles, while they are continuously rising (with no significant changes in the profile shape) in the dome case. All these observations are in line with the present models for radiative instability-driven collapse in stellarators [18]. However, a detail modeling of the power balance and transport at the edge is still required for the assessment of other possible, transport-driven instabilities that could account for the observed density limits under different wall conditions.

Finally, a spiky behavior of the Hα signals was conspicuously observed in NBI heated plasmas under Li-wall conditions. This behavior was seen to have common features with the reported ELM activity in tokamaks and other stellarators, but their phenomenology was not always identified as edge-born phenomena. Instead, the full plasma profile was seen to undergo the oscillation pattern of the Hα signal in some instances. Fig. 8 shows an example for the case of ELM-like events. The spikes in Hα and Li emission, lasting less than 300 μs, are correlated with the fast propagation of a cold pulse which origin seems to be located at the radius where the 8/5 rational is expected (vacuum configuration). Their physical origin and their relation with the presence of bifurcation in transport characteristics is presently under investigation, but some evidence already exists about their correlation with the achievement of high plasmas pressure gradients and fluctuation suppression at the edge in the new, lithium wall scenarios.

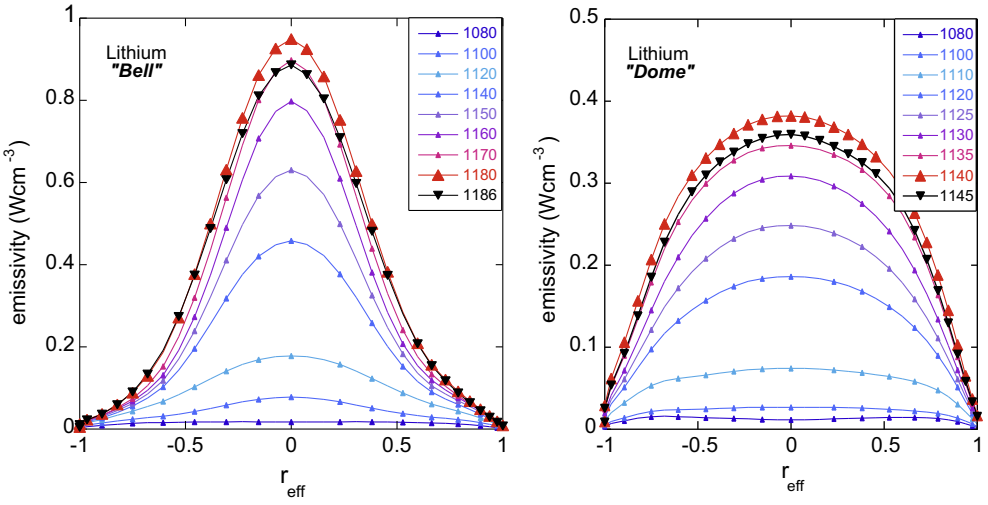

Fig. 7. Radial profile of local emissivities (bolometer data) for the two characteristic plasma profiles found under Li-wall scenarios at several times during a NBI discharge. Left 'bell' type. Right 'dome' type.

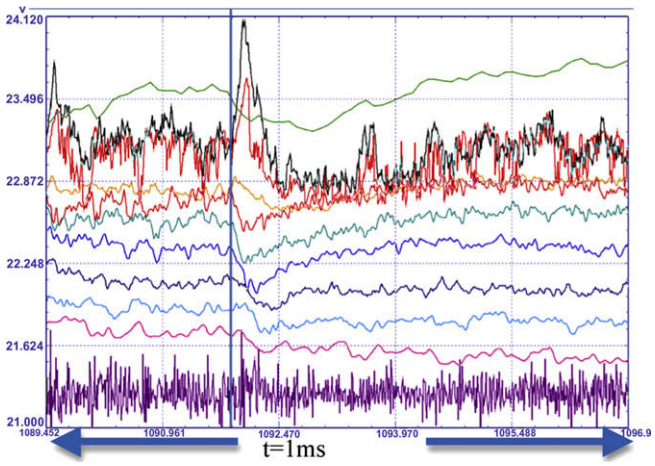

Fig. 8. Details of ELMy behavior in TJ-II. A cold pulse propagates from ECE channel #2 ($r/a = 0.70$) inwards and outwards right after (vertical bar) the spike in particle fluxes (Hα and Li emissions). A velocity of 1 Km/s is deduced form the ECE data. From top to bottom: Li I emission, Hα, diamagnetic loop (slow response), ECE channels #1, 2, 3, 4, 5, 6 and 9 and Mirnov coil.

5. Conclusions

The TJ-II has been operated under lithiated wall conditions, the first time that this technique has ever been applied to a stellarator. Very encouraging results in terms of density control and impurity level have been obtained; even when only partial coverage was achieved. Record values for recycling ($R < 0.2$), plasma density, energy content and confinement were obtained. The development of peaked profiles allowed for the extension of the density limit, which was tentatively ascribed to a local thermal collapse at the edge under the limited NBI power available at present. New techniques for improvement of film homogeneity and careful control of limiter conditions are foreseen in order to improve the results.

Acknowledgment

This work was partially supported by the Spanish Ministry of Science and Innovation, Project number: ENE2006-14577-C04-01/FTN.

References

[1] D.K. Mansfield et al., Nucl. Fus. 41 (2001) 1823.
[2] R. Majeski et al., Phys. Rev. Lett. 97 (2006) 075002.
[3] S.V. Mirnov et al., Plasma Phys. Control. Fus. 48 (2006) 82; S.V. Mirnov et al., these Proceedings.
[4] V. Pericoli-Ridolfini et al., Plasmas Phys. Control. Fus. 49 (2007) S123.
[5] V.A. Evtikhin et al., Plasmas Phys. Control. Fus. 44 (2002) 955.
[6] K. Nishimura et al., J. Nucl. Mater. 337–339 (2005) 431.
[7] H. Wobig, Plasma Phys. Control. Fus. 42 (2000) 931.
[8] F.L. Tabarés, D. Tafalla, et al., J. Nucl. Mater. 266–269 (1999) 1273; D. Tafalla, F.L. Tabarés, ibid 290–293 (2001) 1195.
[9] D. Tafalla, F.L. Tabarés, Vacuum 67 (2002) 393.
[10] F.L. Tabarés et al., Plasma Phys. Control. Fus. 43 (2001) 1023.
[11] F.L. Tabarés et al., in: Proceedings 28th EPS Conference on Plasma Physics and Controlled Fusion, Funchal, Madeira, 2001.
[12] M.A. Pedrosa et al., Plasma Phys. Control. Fus. 49 (2007) B303.
[13] F.L. Tabarés et al., J. Nucl. Mater 313–316 (2003) 839.
[14] S. Kato et al., J. Nucl. Mater 266–269 (1999) 411.
[15] J.P. Allain, D.G. Whyte, J.N. Brooks, Nucl. Fus. 44 (2004) 655.
[16] J. László, W. Eckstein, J. Nucl. Mater. 184 (1991) 22.
[17] J.P. Allain et al., J. Nucl. Mater. 390–391 (2009) 942.
[18] M.A. Ochando, F. Castejón, A.P. Navarro, Nucl. Fus. 37 (1997) 225.